Vehicle sprung mass estimation for rough terrain

Benjamin Pence (bpence@umich.edu), Joseph Hays (joehays@vt.edu), Hosam Fathy (hkf2@psu.edu), Corina Sandu (csandu@vt.edu) and Jeffrey Stein (stein@umich.edu)

This paper provides methods and experimental results for recursively estimating the sprung mass of a vehicle driving on rough terrain. It presents a base-excitation model of vertical ride dynamics which treats the unsprung vertical accelerations, instead of the terrain profile, as the ride dynamics model input. It employs recently developed methods based on polynomial chaos theory and on the maximum likelihood approach to estimate the most likely value of the vehicle sprung mass. The polynomial chaos estimator is compared to benchmark algorithms including recursive least squares, recursive total least squares, extended Kalman filtering, and unscented Kalman filtering approaches. The paper experimentally demonstrates the proposed method. The results of the experimental study suggest that the proposed approach provides accurate outputs and the proposed method is less sensitive to tuning parameters when compared with the benchmark algorithms.

1 Introduction

This paper provides methods and experimental results for recursively estimating the sprung mass of a vehicle driving on rough terrain. An accurate onboard estimate of vehicle mass is valuable to active safety systems as well as chassis and drivetrain controllers. These autonomous systems and controllers schedule gear shifts, actuate brakes, induce steer, schedule fuel injection, warn drivers of rollover susceptibility, etc. Many of them rely on accurate knowledge of the mass of the vehicle to perform optimally. Since vehicle mass can vary significantly from one loading condition to the next, the estimate of vehicle mass needs to be updated online, a constraint which adds its own challenges to the development of the mass estimator.

A significant number of mass estimation algorithms have been developed for *on road* conditions. The authors have surveyed this literature and included a brief summary in the introduction of a paper by Kang, Fathy, and Stein (2008), where another novel algorithm for on road vehicle mass estimation was presented. Much of the scientific literature for vehicle mass estimation uses the longitudinal vehicle dynamics, drivetrain shuffle dynamics, or combined lateral, yaw, and roll dynamics to estimate the vehicle mass. Despite the research successes for on road mass estimation, the *off-road* real-time vehicle mass estimation problem remains relatively unexplored, and existing solutions to this problem remain difficult to apply in practice. One of the main challenges is the fact that the motions introduced by rough terrain are significant enough to make mass estimation based on longitudinal vehicle dynamics infeasible; this rough terrain, however, makes mass estimation based on vertical vehicle dynamics becomes much more viable due to the presence of significant terrain-induced excitations. The overarching goal of this paper is to develop an accurate and fast real-time online mass estimator for vehicles

Report Documentation Page

Form Approved
OMB No. 0704-0188

1. REPORT DATE	2. REPORT TYPE	3. DATES COVERED
01 MAR 2011	**Technical Report**	**27-06-2010 to 28-01-2011**

4. TITLE AND SUBTITLE	5a. CONTRACT NUMBER
Vehicle sprung mass estimation for rough terrain	**W56HZV-04-2-0001**
	5b. GRANT NUMBER
	5c. PROGRAM ELEMENT NUMBER
6. AUTHOR(S)	5d. PROJECT NUMBER
Benjamin Pence; Joseph Hays; Hosam Fathy; Corina Sandu; Jeffrey Stein	5e. TASK NUMBER
	5f. WORK UNIT NUMBER
7. PERFORMING ORGANIZATION NAME(S) AND ADDRESS(ES)	8. PERFORMING ORGANIZATION REPORT NUMBER
University of Michigan,4260 Plymouth Road,Ann Arbor,Mi,48109	**; #21552**
9. SPONSORING/MONITORING AGENCY NAME(S) AND ADDRESS(ES)	10. SPONSOR/MONITOR'S ACRONYM(S)
U.S. Army TARDEC, 6501 East Eleven Mile Rd, Warren, Mi, 48397-5000	**TARDEC**
	11. SPONSOR/MONITOR'S REPORT NUMBER(S)
	#21552

12. DISTRIBUTION/AVAILABILITY STATEMENT

Approved for public release; distribution unlimited

13. SUPPLEMENTARY NOTES

International Journal of Vehicle Design

14. ABSTRACT

This paper provides methods and experimental results for recursively estimating the sprung mass of a vehicle driving on rough terrain. It presents a base-excitation model of vertical ride dynamics which treats the unsprung vertical accelerations, instead of the terrain profile, as the ride dynamics model input. It employs recently developed methods based on polynomial chaos theory and on the maximum likelihood approach to estimate the most likely value of the vehicle sprung mass. The polynomial chaos estimator is compared to benchmark algorithms including recursive least squares, recursive total least squares, extended Kalman filtering, and unscented Kalman filtering approaches. The paper experimentally demonstrates the proposed method. The results of the experimental study suggest that the proposed approach provides accurate outputs and the proposed method is less sensitive to tuning parameters when compared with the benchmark algorithms.

15. SUBJECT TERMS

16. SECURITY CLASSIFICATION OF:			17. LIMITATION OF ABSTRACT	18. NUMBER OF PAGES	19a. NAME OF RESPONSIBLE PERSON
a. REPORT	b. ABSTRACT	c. THIS PAGE			
unclassified	**unclassified**	**unclassified**	**Public Release**	**20**	

negotiating rough terrain, and to demonstrate its viability through experimental data collected from an actual vehicle.

A number of excellent papers and patents have explored the use of the ride dynamics for vehicle mass estimation. Often, these methods assume that the terrain profile is known, estimated, or measured (Blanchard, Sandu and Sandu (2009a,b,2010), Best and Gordon (1998), Huh et al. (2007), Kim and Ro (2000), Lin and Kortum (1992), and Shimp (2008)). Others assume that the suspension is equipped with an active or semi-active force actuator which provides a known suspension force (Ohsaku and Nakai (2000), Rajamani and Hedrick (1995), and Song, Ahmadian, and Southward (2005)). Finally, Tal and Elad (1999) analyzed the dynamics in the frequency domain to reveal important resonance frequencies related to the value of the sprung mass and suspension spring constant. Unlike the methods above, this paper seeks an estimation algorithm which does not require *a priori* knowledge or explicit measurement or estimation of road terrain and does not require active or semi-active suspension force actuation. This study also aims at using a minimal/inexpensive sensor set to achieve the mass estimation.

The proposed solution presented in this paper adopts a *base excitation* approach to real-time off-road vehicle mass estimation. It introduces the base excitation model which treats the vertical accelerations at the four unsprung masses as measured inputs to sprung vehicle dynamics and uses the governing equations of these sprung vehicle dynamics for mass estimation. This approach furnishes estimation schemes that do not require *a priori* knowledge, measurement, or estimation of the terrain. This paper also explores potential benefits of using a polynomial chaos based approach (Blanchard, Sandu and Sandu (2009a,b,2010)) for recursive parameter estimation (Pence, Fathy and Stein (2010) and Pence, Fathy and Stein (2011)) and compares it with benchmark algorithms such as regression approaches and state-filtering approaches.

This paper is structured as follows. The following section presents the derivation of the full vehicle base excitation model used in this work's proposed estimator. The proposed recursive polynomial chaos, and benchmark regressor and filtering based estimators are presented in Sections 3–5, respectively. Section 6 presents the results related to investigating the degree to which a vehicle's pitch dynamics contribute to the mass estimation problem within the context of an estimator that uses a base-excitation based model. Section 7 details the experimental setup followed by comparisons of the experimental results between the proposed recursive Polynomial Chaos based estimator and the regressor and filtering methods in Sections 8–9, respectively. Concluding remarks are in Section 10.

2 Base Excitation Full Car Ride Model

Vehicle dynamics literature commonly uses a seven degree of freedom system to model the general behavior of a vehicle's ride dynamics. An illustration of this model is provided in Figure 1. The seven degrees of freedom include the vertical $z_{s,cg}$, roll θ_s, and pitch φ_s motion of the sprung mass, as well as the vertical motions $z_{u,fl}, z_{u,fr}, z_{u,rl}, z_{u,rr}$ of the four unsprung masses.

The motions $z_{g,fl}, z_{g,fr}, z_{g,rl}, z_{g,rr}$ of the four tire surfaces at the ground are the inputs to the seven degree of freedom model.

The base-excitation concept treats the unsprung mass motions instead of the terrain as the model input (as illustrated in Figure 2). This methodology is adopted from the vibrations literature (Inman (2001)) and has been used for mass estimation by Pence, Fathy and Stein (2009a and 2009b) and Song, Ahmadian and Southward (2005), but these methods only considered a quarter-car model

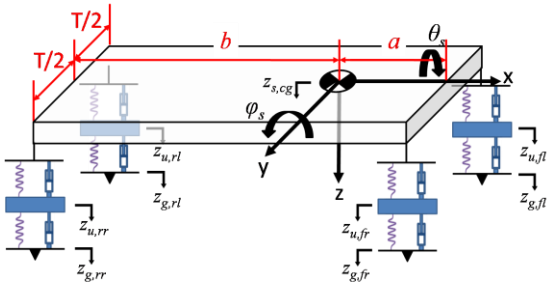

Figure 1: Seven degree of freedom model of vehicle ride dynamics.

of the vehicle. As a key difference from the traditional full-car ride model, the full-car base excitation model treats the vertical unsprung mass accelerations $\ddot{z}_{u,fl}, \ddot{z}_{u,fr}, \ddot{z}_{u,rl}, \ddot{z}_{u,rr}$, the longitudinal velocity U in the x-direction with respect to body fixed axes, and the sprung mass pitch velocity $\dot{\varphi}_s$ as measured model inputs. (A reduced order model at the end of this section will require only the unsprung mass accelerations as the system inputs). The "dot" notation denotes the derivative with respect to time. The resulting system models the dynamics of the sprung mass in the following three degrees of freedom: vertical $z_{s,cg}$, pitch φ_s, and roll θ_s. The base excitation model is shown in Figure 3.

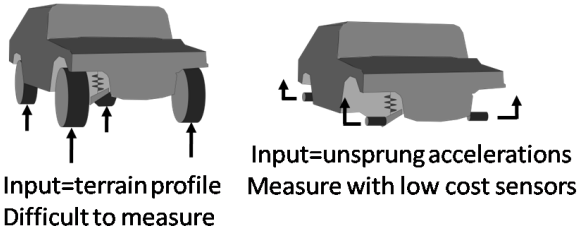

Figure 2: Base excitation concept

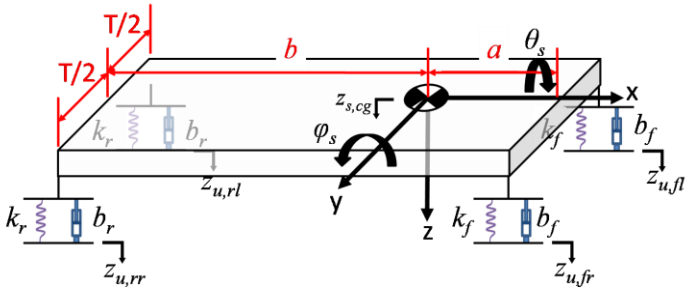

Figure 3: Base excitation model of full car ride dynamics.

The base excitation model has a number of key benefits for vehicle mass estimation compared with the traditional full-car ride model: the model avoids requiring knowledge of the values of the unsprung masses, tire stiffness and damping, and, most importantly, terrain profile. Also, the

reduced degrees of freedom result in fewer model states and hence, less computational complexity.

This paper makes the following simplifying assumptions:

1. Negligible yaw velocity ($\dot{\psi} = 0$)
2. Negligible lateral velocity ($V = 0$)
3. Small pitch φ and roll θ angles
4. Linear suspension elements
5. Left-right symmetry in suspension elements, *e.g.*, the front left spring stiffness is the same as the front right spring stiffness, *e.g.*, $k_{fl} = k_{fr} =: k_f$.
6. The c.g. is at half the track width $T/2$, a known distance a behind the front axle of the vehicle, and a distance b forward from the rear axle. The wheelbase length is $a + b$.

Applying Euler's laws of motion to the sprung mass of Figure 3 results in the following equations which govern the dynamic behavior of the base excitation full car model:

$$\begin{aligned} z - equation&: m\left(\ddot{z}_{s,cg} - \dot{\varphi}_s U\right) = F_z \\ \varphi - equation&: J_\varphi \ddot{\varphi}_s = M_\varphi \\ \theta - equation&: J_\theta \ddot{\theta}_s = M_\theta \end{aligned} \tag{1}$$

Here, F_z is the net downward force acting on the sprung mass, M_φ is the net moment or torque about the y axis, and M_θ is the moment acting about the x axis. These forces and moments are produced via the suspension elements as follows:

$$F_z \coloneqq \sum_{i=fl,fr,rl,rr} F_i \tag{2}$$

$$M_\varphi \coloneqq -\left(F_{fl} + F_{fr}\right)a + \left(F_{rl} + F_{rr}\right)b \tag{3}$$

$$M_\theta \coloneqq -\frac{T}{2}\left(F_{fl} + F_{rl}\right) + \frac{T}{2}\left(F_{fr} + F_{rr}\right) \tag{4}$$

The forces $F_i,\ i = fl, fr, rl, rr$ are due to suspension deflections and velocities and are calculated by

$$F_{fl} \coloneqq k_f\left(z_{u,fl} - z_{s,cg} + a\varphi_s + \frac{T}{2}\theta_s\right) + b_f\left(\dot{z}_{u,fl} - \dot{z}_{s,cg} + a\dot{\varphi}_s + \frac{T}{2}\dot{\theta}_s\right) \tag{5}$$

$$F_{fr} \coloneqq k_f\left(z_{u,fr} - z_{s,cg} + a\varphi_s - \frac{T}{2}\theta_s\right) + b_f\left(\dot{z}_{u,fr} - \dot{z}_{s,cg} + a\dot{\varphi}_s - \frac{T}{2}\dot{\theta}_s\right) \tag{6}$$

$$F_{rl} \coloneqq k_r\left(z_{u,rl} - z_{s,cg} - b\varphi_s + \frac{T}{2}\theta_s\right) + b_r\left(\dot{z}_{u,rl} - \dot{z}_{s,cg} - b\dot{\varphi}_s + \frac{T}{2}\dot{\theta}_s\right) \tag{7}$$

$$F_{rr} \coloneqq k_r\left(z_{u,rr} - z_{s,cg} - b\varphi_s - \frac{T}{2}\theta_s\right) + b_r\left(\dot{z}_{u,rr} - \dot{z}_{s,cg} - b\dot{\varphi}_s - \frac{T}{2}\dot{\theta}_s\right). \tag{8}$$

For convenience, this section defines the following terms:

$$z_{u,cg} \coloneqq \frac{b\left(z_{u,fl} + z_{u,fr}\right) + a\left(z_{u,rl} + z_{u,rr}\right)}{2(a+b)} \tag{9}$$

$$\varphi_u \coloneqq \frac{-\left(z_{u,fl} + z_{u,fr}\right) + \left(z_{u,rl} + z_{u,rr}\right)}{2(a+b)} \tag{10}$$

$$Z \coloneqq z_{s,cg} - z_{u,cg} \tag{11}$$

$$\Phi \coloneqq \varphi_s - \varphi_u \tag{12}$$

The terms $z_{u,cg}$ and φ_u can be interpreted as the average vertical position and average pitch of the unsprung masses. Then, the terms Z and Φ can be interpreted as the average vertical and angular displacements of the sprung mass relative to the unsprung masses.

Given definitions (2) Through (12), the z and φ equations of (1) can be written as:

$$\begin{aligned} z - equation{:}\ m\ddot{Z} &= F_z + m\left(\dot{\varphi}_s U - \ddot{z}_{u,cg}\right) \\ \varphi - equation{:}\ J_\varphi \ddot{\Phi} &= M_\varphi - J_\varphi \ddot{\varphi}_u \end{aligned} \tag{13}$$

The vertical force F_z and pitch moment M_φ can also be written as functions of the terms defined in (9) through (12):

$$F_z = -2\left(k_f + k_r\right)Z - 2\left(b_f + b_r\right)\dot{Z} + 2\left(ak_f - bk_r\right)\Phi + 2\left(ab_f - bb_r\right)\dot{\Phi} \tag{14}$$

$$\begin{aligned} M_\varphi = {} & 2\left(ak_f - bk_r\right)Z + 2\left(ab_f - bb_r\right)\dot{Z} - 2\left(a^2k_f + b^2k_r\right)\Phi \\ & - 2\left(a^2b_f + b^2b_r\right)\dot{\Phi} \end{aligned} \tag{15}$$

Equations (13) through (15) are independent of the roll motion of the sprung mass. As a result, the roll dynamics can be neglected without sacrificing accuracy in the calculation of the vertical and pitch motion. This result enables a lower order (and less computationally expensive) estimator.

The state space representation of Equations (13) through (15) is as follows:

$$\begin{aligned} \begin{bmatrix} \dot{x}_1 \\ \dot{x}_2 \\ \dot{x}_3 \\ \dot{x}_4 \end{bmatrix} = {} & \begin{bmatrix} 0 & 1 & 0 & 0 \\ \frac{-2\left(k_f + k_r\right)}{m} & \frac{-2\left(b_f + b_r\right)}{m} & \frac{2\left(ak_f - bk_r\right)}{m} & \frac{2\left(ab_f - bb_r\right)}{m} \\ 0 & 0 & 0 & 1 \\ \frac{2\left(ak_f - bk_r\right)}{J_\varphi} & \frac{2\left(ab_f - bb_r\right)}{J_\varphi} & \frac{-2\left(a^2k_f + b^2k_r\right)}{J_\varphi} & \frac{-2\left(a^2b_f + b^2b_r\right)}{J_\varphi} \end{bmatrix} \begin{bmatrix} x_1 \\ x_2 \\ x_3 \\ x_4 \end{bmatrix} \\ & + \begin{bmatrix} 0 & 0 & 0 & 0 & 0 \\ \frac{-b}{2(a+b)} & \frac{-b}{2(a+b)} & \frac{-a}{2(a+b)} & \frac{-a}{2(a+b)} & 1 \\ 0 & 0 & 0 & 0 & 0 \\ \frac{1}{2(a+b)} & \frac{1}{2(a+b)} & \frac{-1}{2(a+b)} & \frac{-1}{2(a+b)} & 0 \end{bmatrix} \begin{bmatrix} \ddot{z}_{u,fl} \\ \ddot{z}_{u,fr} \\ \ddot{z}_{u,rl} \\ \ddot{z}_{u,rr} \\ \dot{\varphi}_s U \end{bmatrix} \end{aligned} \tag{16}$$

The states are $x_1 = Z$, $x_2 = \dot{Z}$, $x_3 = \Phi$, and $x_4 = \dot{\Phi}$. The set of dynamic state equations in (16) govern the motion of the base excitation system shown in (16). These dynamic equations can be combined with the estimation techniques of this paper for a potential solution to vehicle mass estimation. There are a few factors, however, that motivate reducing this set of state equations/sensor inputs in (16) to a lower dimensional set. The first motivating factor is the desire to reduce the computational complexity of the estimator. This is important for online/onboard algorithms which may have limited access to memory and computational resources on an onboard computer. The second factor is motivated by the desire to reduce the number of sensors required to perform the online estimation. Based on these motivating factors, this section derives a reduced order model, but will also note that the lower order estimator also has a lower fidelity than an estimator which uses the higher-order set of state equations given in

(16). For example, simulation results in Section 6 show that an improved estimate is obtained by using (16) compared to the reduced order model when the vehicle experiences large pitch values.

To reduce the set of state equations/sensor inputs to a lower dimensional set, this paper notes that in many vehicles, the coupling term between the vertical and pitch dynamics may be negligible. In Equation (16), the vertical and pitch dynamics are coupled by the terms $2(ak_f - bk_r)/m$, $2(ab_f - bb_r)/m$, $2(ak_f - bk_r)/J_\varphi$ and $2(ab_f - bb_r)/J_\varphi$. In some cases, the numerator of each term is small, and the denominator is large. For example, if $ak_f = bk_r$, and $ab_f = bb_r$ the numerators are zero and there is no coupling between the vertical and pitch dynamics. When these coupling terms are not weak, a stronger assumption is required, which is to assume that the pitch motion of the vehicle is negligible. Either of these assumptions enable decoupling of the pitch and vertical dynamics, and the set of equations given in (16) can be reduced to the following second order state equations that govern the vertical motion of the sprung mass:

$$\begin{bmatrix}\dot{x}_1\\ \dot{x}_2\end{bmatrix} = \begin{bmatrix}0 & 1\\ \dfrac{-2(k_f+k_r)}{m} & \dfrac{-B_z}{m}\end{bmatrix}\begin{bmatrix}x_1\\ x_2\end{bmatrix} + \begin{bmatrix}0\\ -1\end{bmatrix}\mathrm{u}$$

$$\mathrm{u} = \begin{bmatrix}0 & 0 & 0 & 0\\ \dfrac{\mathrm{b}}{2(\mathrm{a}+\mathrm{b})} & \dfrac{\mathrm{b}}{2(\mathrm{a}+\mathrm{b})} & \dfrac{\mathrm{a}}{2(\mathrm{a}+\mathrm{b})} & \dfrac{\mathrm{a}}{2(\mathrm{a}+\mathrm{b})}\end{bmatrix}\begin{bmatrix}\ddot{z}_{u,fl}\\ \ddot{z}_{u,fr}\\ \ddot{z}_{u,rl}\\ \ddot{z}_{u,rr}\end{bmatrix} \quad (17)$$

Here, $B_z = 2(b_f + b_r)$. The measured output y is the vertical acceleration $\ddot{z}_{s,cg}$ of the sprung mass at the center of gravity location, and the output equation is as follows:

$$y = \begin{bmatrix}\dfrac{-2(k_f+k_r)}{m} & \dfrac{-B_z}{m}\end{bmatrix}\begin{bmatrix}x_1\\ x_2\end{bmatrix} \quad (18)$$

The known or measured variables/parameters of equations (17)–(18) are the four unsprung mass accelerations, the distances from the axles to the sprung mass c.g. location, and the front and rear spring stiffness values. The unknowns parameters/variables include the value of the vehicle sprung mass m, the damping term B_z, and the state variables x_1 and x_2.

The estimation algorithms are discussed in the following sections.

3 Polynomial Chaos and Maximum Likelihood

Pence, Fathy, and Stein (2010 and 2011) have developed a recursive maximum likelihood estimator for state-space systems using polynomial chaos theory. This estimator builds on the polynomial chaos technique for modeling multibody dynamic systems with uncertainties developed by Sandu, Sandu, and Ahmadian (2006a and 2006b) and extends the batch maximum *a posteriori* estimator developed by Blanchard, Sandu, and Sandu (2009a,b,2010) to applications that require recursive estimation. Existing research has explored the use of recursive polynomial chaos based algorithms for vehicle mass estimation (Pence, Fathy, and Stein (2009b) and Shimp

(2008)). The study presented here, however, uses an algorithm that estimates parameters based on an *integrated* cost function which is different from the previous approaches which used an algorithm that updates parameter estimates based on an *instantaneous* cost function. The earlier work by Pence, Fathy, and Stein (2009b) showed that estimators based on the *instantaneous* cost criteria resulted in estimates having significant variance. Another difference between this and the earlier work is that the earlier research was directed at quarter-car suspension models.

The polynomial chaos approach is applied directly to the system of Equations (17)–(18). Because the system of Equations (17)–(18) is linear, the Galerkin approach (discussed in Pence, Fathy, and Stein (2010 and 2011)) can be applied. To apply the polynomial chaos based algorithms, the unknown parameters are treated as random variables. The polynomial chaos algorithm requires upper and lower bounds on the unknown parameters which can be inferred from prior knowledge. This paper assumes that the true values of the unknown parameters could potentially be any values between the lower and upper bounds with equal probability, i.e., it assumes that the prior distributions are uniform. With known upper and lower bounds, the random variables representing the unknown mass and damping terms can be written as functions of independently identically distributed (iid) polynomial chaos variables ξ_m and ξ_B, each of which are uniformly distributed over the interval [-1, 1]:

$$\begin{aligned} m &= \mu_m + v_m \xi_m \\ B_z &= \mu_B + v_B \xi_B \end{aligned} \tag{19}$$

Here, μ_m and μ_B are respectively the known mean values of the mass m and damping B_z random variables. The terms v_m and v_B are the known maximum variation values of m and B_z respectively from the mean values μ_m and μ_B; *e.g.*, $v_m = m_{upperLimit} - \mu_m$ where $m_{upperLimit}$ is the largest possible numerical value of the mass m. The goal of polynomial chaos based estimation is to estimate the most likely realizations of ξ_m and ξ_B and hence, by (19), the most likely values of the unknown mass m and damping term B_z.

Applying the Galerkin method of polynomial chaos theory to the system of Equations (17)–(18) (with the unknown parameters m and B_z replaced by their polynomial chaos counterparts given in (19)) results in the following set of deterministic state equations:

$$\dot{X} = \begin{bmatrix} \mathbf{0}_{r\times r} & \boldsymbol{I}_{r\times r} \\ A_{21} & A_{22} \end{bmatrix} X + \begin{bmatrix} \mathbf{0}_r \\ -1 \\ \mathbf{0}_{r-1} \end{bmatrix} u \tag{20}$$

Here, $\mathbf{0}_k, k \in \{r \times r, r, r-1\}$ is a matrix/vector of zeros having dimension k, the identity matrix $\boldsymbol{I}_{r\times r}$ has dimensions $r \times r$, and $r = (S^2 + 3S + 2)/2$ where S is the user-selected maximum polynomial chaos order, ($S = 6$ in the experiments of this paper). The state vector $X \in \mathbb{R}^{2r}$ is a vector of polynomial chaos expansion coefficients. Finally, the matrices $A_{21} \in \mathbb{R}^{r\times r}$ and $A_{22} \in \mathbb{R}^{r\times r}$ are defined as follows:

$$A_{21} \coloneqq A_{diag} \begin{bmatrix} \langle \Phi_1, Q\Phi_1 \rangle & \langle \Phi_1, Q\Phi_2 \rangle & \cdots & \langle \Phi_1, Q\Phi_r \rangle \\ \langle \Phi_2, Q\Phi_1 \rangle & \langle \Phi_2, Q\Phi_2 \rangle & & \langle \Phi_2, Q\Phi_r \rangle \\ \vdots & & \ddots & \vdots \\ \langle \Phi_r, Q\Phi_1 \rangle & \langle \Phi_r, Q\Phi_2 \rangle & \cdots & \langle \Phi_r, Q\Phi_r \rangle \end{bmatrix}, Q = \frac{-2(k_f + k_r)}{\mu_m + v_m \xi_m} \tag{21}$$

$$A_{22} \coloneqq A_{diag} \begin{bmatrix} \langle \Phi_1, G\Phi_1 \rangle & \langle \Phi_1, G\Phi_2 \rangle & \cdots & \langle \Phi_1, G\Phi_r \rangle \\ \langle \Phi_2, G\Phi_1 \rangle & \langle \Phi_2, G\Phi_2 \rangle & & \langle \Phi_2, G\Phi_r \rangle \\ \vdots & & \ddots & \vdots \\ \langle \Phi_r, G\Phi_1 \rangle & \langle \Phi_r, G\Phi_2 \rangle & \cdots & \langle \Phi_r, G\Phi_r \rangle \end{bmatrix}, G = \frac{-(\mu_B + v_B \xi_B)}{\mu_m + v_m \xi_m} \tag{22}$$

$$A_{diag} \coloneqq \begin{bmatrix} \langle \Phi_1, \Phi_1 \rangle^{-1} & 0 & \cdots & 0 \\ 0 & \langle \Phi_2, \Phi_2 \rangle^{-1} & & 0 \\ & \vdots & \ddots & \vdots \\ 0 & 0 & \cdots & \langle \Phi_r, \Phi_r \rangle^{-1} \end{bmatrix} \tag{23}$$

The polynomial chaos based estimator is asymptotically stable if the eigenvalues of the state transition matrix in Equation (20) have negative real parts. For the base excitation model, stability is guaranteed when the lower bounds on the parameter prior distributions are greater than zero. The multivariate polynomials $\Phi_k, k = 1,2, \dots, r$ are functions of the Legendre polynomials (Poularikas (1999)) $\phi_i(\xi_m), i = 0,1, \dots, S$ and $\phi_j(\xi_B), j = 0,1, \dots, S$ as follows:

$$\Phi_k = \phi_i(\xi_m)\, \phi_j(\xi_B), \qquad k = i\left(S + \frac{3-i}{2}\right) + j + 1, \qquad i = 0,1, \dots, S, \quad j = 0,1, \dots, S - i \tag{24}$$

The inner products $\langle f(\xi_m, \xi_B), g(\xi_m, \xi_B) \rangle$ are defined as follows:

$$\langle f(\xi_m, \xi_B), g(\xi_m, \xi_B) \rangle \coloneqq \int_{-1}^{1} \int_{-1}^{1} g(\xi_m, \xi_B) f(\xi_m, \xi_B) d\xi_m d\xi_B \tag{25}$$

Since the integrals are evaluated over the event space of the random variables, the inner product $\langle f(\xi_m, \xi_B), g(\xi_m, \xi_B) \rangle$ is a known deterministic quantity; as a result, Equation (20) is a deterministic set of state equations that can be solved numerically to determine the value of the state vector X. Also, since the multivariate polynomials $\Phi_k, k = 1,2, \dots, r$ are orthogonal with respect to the inner product in Equation (25), the matrix A_{diag} is well defined.

Following the concepts of polynomial chaos theory, the states x_1 and x_2 of Equation (17) are functions of the random variables ξ_m and ξ_B, and are related to the state vector X of Equation (20) through a polynomial chaos expansion approximation:

$$\begin{bmatrix} x_1 \\ x_2 \end{bmatrix} \approx PX, \qquad P \coloneqq \begin{bmatrix} \Phi_1 & \cdots & \Phi_r & \mathbf{0}_{1\times r} \\ \mathbf{0}_{1\times r} & & \Phi_1 & \cdots \quad \Phi_r \end{bmatrix} \tag{26}$$

This approximation becomes exact in the least squares sense as $S \to \infty$ (Ghanem and Spanos (1991)). Substituting Equations (26) and (19) into (18) results in the polynomial chaos approximation output $\hat{y}$ which is a function of the unknown variables ξ_m and ξ_B.

$$\hat{y} \approx \begin{bmatrix} \frac{-2(k_f + k_r)}{\mu_m + v_m \xi_m} & \frac{-(\mu_B + v_B \xi_B)}{\mu_m + v_m \xi_m} \end{bmatrix} PX \tag{27}$$

The output $\hat{y}$ is not an output *trajectory* but rather an output *process* or family of trajectories. From (27), one can see that given realizations of ξ_m and ξ_B, $\hat{y}$ collapses to an output trajectory. The goal of recursive maximum likelihood is to determine the realizations of ξ_m and ξ_B that make $\hat{y}$ most like the measured output y in some sense. This is done by selecting ξ_m and ξ_B so

that they optimize the likelihood function (assuming zero mean Gaussian measurement noise with variance ${\sigma_k}^2$):

$$\mathcal{L}(\xi_m, \xi_B | y) \propto exp\left\{ -\sum_{k=0}^{N} \frac{\left(y(t_k) - \hat{y}(t_k, \xi_m, \xi_B)\right)^2}{2{\sigma_k}^2} \right\} \tag{28}$$

Pence, Fathy, and Stein (2010 and 2011) developed techniques for recursively calculating estimates of the unknown parameters that recursively seek to optimize the likelihood function (28). The key limitation of the polynomial chaos based method is the fact that the polynomial chaos approximation is only exact in the limiting sense as $S \to \infty$ which is not numerically feasible. The authors have found, as a rule of thumb, that $S \geq 6$ is a good approximation for this mass estimation problem. A general procedure to determine an acceptable value for S is to start with a small value for S and then increase the value until the change in the resulting estimates is negligible.

4 Regressor Model Based Estimation Methods

An alternative approach to using polynomial chaos based estimation is to use regressor-model based algorithms such as recursive least squares (RLS) (Ioannou and Sun (1996)) or recursive total least squares (RTLS) (*e.g.*, Kubus, Kroger, and Wahl (2008)). Under certain Gaussian measurement noise assumptions, and if the states x_1 and x_2 of Equations (17) are measured explicitly, RLS methods can potentially produce unbiased estimates. Unfortunately, full-state measurements require measuring suspension displacements and velocities at each corner of the vehicle, as well as the sprung mass acceleration. This paper follows Fathy, Kang, and Stein's (2008) method in using pre-filtering as a precursor to mass estimation. Such pre-filtering has two very attractive advantages, namely, (a) it allows the estimation process to focus on those frequencies where inertial dynamics are more visible, and (b) it makes it possible to estimate sprung mass using sprung and unsprung mass accelerations, without any need to use additional sensors for displacement and velocity.

RLS and RTLS algorithms rely on the regressor model shown in Equation (29) and cannot be applied directly to state-space systems such as the system modeled by Equations (17)–(18).

$$y_R = {\phi_R}^T \theta_R \tag{29}$$

The term y_R is the measured *regressor output*, the term ϕ_R is the *regressor vector* which is also known/measured, and the term θ_R is the *unknown parameter vector*. For vehicle mass estimation, the regressor model can be derived from the output equation, Equation (18). Then, the regressor output y_R is $-2(k_f + k_r)x_1$, the regressor vector ϕ_R is $[y \quad x_2]^T$, and the unknown parameter vector θ_R is$[m \quad B_z]^T$, *i.e.*,

$$-2(k_f + k_r)x_1 = [y \quad x_2] \begin{bmatrix} m \\ B_z \end{bmatrix} \tag{30}$$

The regressor output y_R and regressor vector ϕ_R must only contain known/measured variables, but the states x_1 and x_2 are not measured. To address this problem, this paper applies Laplace-domain filtering to obtain a regressor model in which both y_R and ϕ_R only contain

known/measured values. These Laplace domain filters act as pseudo-integrators to obtain estimates of velocity and displacement from measurements of suspension acceleration. Assuming zero initial conditions for the states x_1 and x_2, the system of equations given in (17)–(18) can be represented in the Laplace-domain by the following transfer function:

$$\frac{Y(s)}{U(s)} = \frac{B_z s + 2\left(k_f + k_r\right)}{ms^2 + B_z s + 2\left(k_f + k_r\right)} \tag{31}$$

In (31), s is the Laplace operator, $Y(s)$ is the Laplace transform of the sprung mass accelerations y, and $U(s)$ is the Laplace transform of the input u. Alternatively, (31) can be written as follows:

$$-2\left(k_f + k_r\right)(Y(s) - U(s)) = ms^2 Y(s) + B_z s(Y(s) - U(s)) \tag{32}$$

Dividing both sides of (32) by $\Lambda(s)$, results in the following filtered regressor model:

$$-2\left(k_f + k_r\right)\frac{(Y(s) - U(s))}{\Lambda(s)} = \begin{bmatrix} \frac{s^2 Y(s)}{\Lambda(s)} & \frac{s(Y(s) - U(s))}{\Lambda(s)} \end{bmatrix} \begin{bmatrix} m \\ B_z \end{bmatrix} \tag{33}$$

The user-selected denominator $\Lambda(s)$ should be a polynomial function of s that is at least second order to ensure that the transfer functions in (33) are proper. The polynomial $\Lambda(s)$ must also have complex roots with negative real parts to guarantee stability. Reverting back to the time domain, the regressor model shown in Equation (33) becomes:

$$-2\left(k_f + k_r\right)\left\{\frac{1}{\Lambda(p)}\right\}(y - u) = \begin{bmatrix} \left\{\frac{p^2}{\Lambda(p)}\right\} y & \left\{\frac{p}{\Lambda(p)}\right\}(y - u) \end{bmatrix} \begin{bmatrix} m \\ B_z \end{bmatrix} \tag{34}$$

The term $\{1/\Lambda(p)\}(y - u)$ represents the time domain signal $y - u$ filtered by the Laplace domain transfer function $\{1/\Lambda(s)\}$. The use of the operator p instead of s is to distinguish between the time and Laplace domains.

Equation (34) contains only known/measured variables in the regressor output $y_R = -2\left(k_f + k_r\right)\{1/\Lambda(p)\}(y - u)$ and regressor vector $\phi_R = [\{p^2/\Lambda(p)\}y \quad \{p/\Lambda(p)\}(y - u)]^T$. The only unknown variables in (34) are the elements of the parameter vector $\theta_R = [m \quad B_z]^T$. Therefore, Equation (34) is a valid model for these regressor model based algorithms. However, two significant problems arise when using Equation (34). First, both the regressor output y_R and regressor vector ϕ_R contain measurements of both y and u. Thus, the noise in the output y_R and regressor vector ϕ_R is correlated. This leads to biased estimates when using recursive least squares algorithms. This approach was explored in a simulation study by Pence, Fathy, and Stein (2008a). Total least squares regression can potentially lead to less biased estimates (Moon and Stirling (2000)). However, a second problem with using Equation (34) affects both least squares and total least squares methods: these methods are both sensitive to the user-selected denominator $\Lambda(s)$. As the experimental validation section will show, slightly different tunings of $\Lambda(s)$ lead to significantly different estimates of the unknown parameters, and tunings that are optimal for one terrain are not necessarily optimal for another.

5 Filtering Methods

Filtering algorithms, such as the Extended Kalman Filter (EKF), Unscented Kalman Filter (UKF) (Simon (2006)), particle filter (Ristic, Maskell and Gordon (2004)), etc., can estimate both the states and unknown parameters of state space systems. Unlike the estimation methods discussed in the paragraphs above which require a regressor model, the filtering algorithms can be applied to state space systems such as the base excitation system of Equations (17)–(18). First, however, the state vector must be augmented to include estimates of the unknown parameters. This augmented set of state and output equations for the base excitation system of Equations (17)–(18) is given as follows:

$$\begin{bmatrix} \dot{x}_1 \\ \dot{x}_2 \\ \dot{x}_3 \\ \dot{x}_4 \end{bmatrix} = \begin{bmatrix} x_2 \\ -\dfrac{2\left(k_f + k_r\right)}{x_3} x_1 - \dfrac{x_4}{x_3} x_2 - u \\ 0 \\ 0 \end{bmatrix} \tag{35}$$

$$y = -\frac{2\left(k_f + k_r\right)}{x_3} x_1 - \frac{x_4}{x_3} x_2 \tag{36}$$

The state x_3 is an estimate of the unknown value of the vehicle sprung mass m, and the state x_4 estimates the unknown damping term B_z. The filtering methods discussed above can be applied to this augmented system of Equations (35) and (36). This augmented system has a higher dimension and is significantly more nonlinear than the (linear) system of Equations (17)–(18). Similar to the regressor model approaches, the filtering methods are more difficult to tune than the proposed polynomial chaos approach. The filtering methods have a large number of user-defined tuning variables: the 4×4 process noise covariance matrix, the measurement noise variance, the initial conditions for the 4×4 estimate covariance matrix, and the initial conditions for the state vector (a total of at least 25 scalar tuning parameters). Despite being difficult to tune, the EKF is especially attractive because of its low computational demand compared with the polynomial chaos approach and even the UKF and particle filter.

6 Pitch dynamics investigation

In Section 2, the 2nd order base-excitation model Equation (17) was developed assuming the pitch dynamics had negligible contribution to the estimation of the sprung mass. In an effort to investigate the validity of this assumption, a maximum likelihood polynomial chaos mass estimator was developed based on the 4th order model in (16) that includes the pitch dynamics. The performance of the two estimators was compared via a numerical simulation of a nonlinear seven degree-of-freedom full vehicle model, developed by Li, Sandu, and Sandu (2005), that was parameterized similar to the 2001 Nissan Altima, GXE sedan (as used in Section 7). The simulation induced a relatively large pitch (about 8 degrees) in the vehicle by driving it over a 30 centimeter bump. Figure 4 shows the relative performance of the two estimators. The 4th order estimator is shown in (a) and converged to an answer within less than 1% of the actual vehicle's

mass. However, the performance of the 2nd order estimator, shown in (b), resulted in an estimate with about a 12% error.

This study implies that inclusion of the pitch dynamics in the estimator can increase the accuracy of the estimates when larger pitch is experienced. The computation cost of the added pitch dynamics was roughly 4x that of the simpler 2nd order estimator; this corresponds with the $O(n^2)$ different between the size of the two models. Therefore, an additional degree-of-freedom is available in choosing which estimator to implement. If sufficient computational resources are available and reasonably large pitches are expected then the 4th order estimator is recommended.

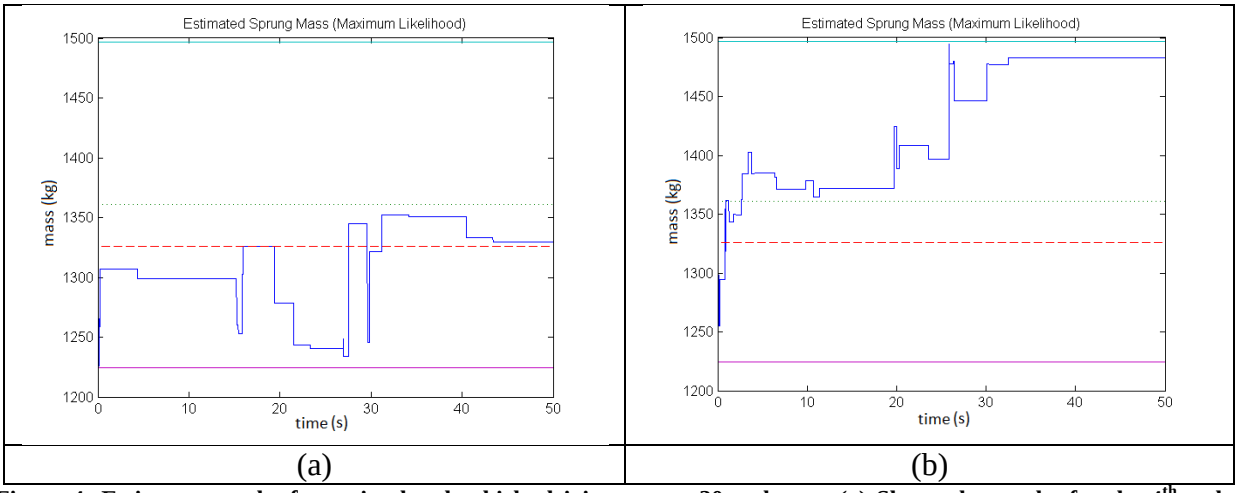

Figure 4: Estimator results for a simulated vehicle driving over a 30cm bump. (a) Shows the results for the 4th order Maximum Likelihood estimator that includes the pitch dynamics. (b) Shows the results for the proposed 2nd order Maximum Likelihood estimator that does *not* include the pitch dynamics.

The remainder of this paper is dedicated to the experimental validation of the methods of this paper.

7 Experimental Setup

The vehicle used for the experiments of this paper was a 2001 Nissan Altima, GXE sedan. The accelerometers used to measure both the sprung and unsprung mass accelerations were Silicon Designs, Inc. single-axis accelerometers, model 2210-005. Unsprung mass accelerometers were attached to the suspension struts (Figure 5) using J.B. Weld® epoxy. The sprung mass accelerometer was attached to the base of the cup holder between the front seats (Figure 6) using Duro® super-glue. The data acquisitioning system was a National Instruments® model NI USB-6221. Data samples were taken at a 500 Hz or 1 kHz rate, filtered using a low pass filter as discussed later, and then downsampled to a 100 Hz rate. The accelerometers were connected to the acquisitioning system in differential mode.

A Proform® 67650 Vehicle Scale System was used to measure the total vehicle weight (including the driver and acquisitioning equipment weight), which was found to be 1460 kg (3220 lbs). This Vehicle Scale System also determined the Center of Gravity (cg) location to be a distance of 62% of the wheelbase length (2.59 m) forward from the rear axle. The tires and

wheels were also weighed and found to have a total mass of 70 kg (150 lbs). The remaining mass of the unsprung components (hub, suspension, axle, etc.) was estimated to be 94 kg (210 lbs) based on shipping weight calculations published on an internet website: Amazon.com™. These unsprung components with their associated shipping weight estimates are listed in Table 1. Based on the measurements of the tire and wheel weight and the estimated value of the remaining unsprung mass, the total sprung mass was 1296 kg (2860 lbs).

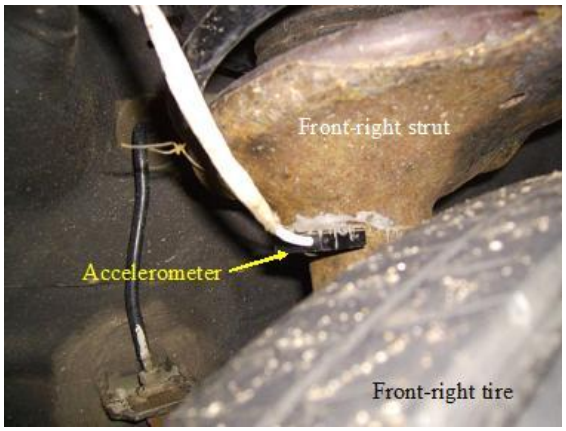

Figure 5: Placement of the unsprung accelerometer.

Figure 6: Location of sprung mass accelerometer.

Table 1: Mass of unsprung suspension components.

Unsprung Suspension Components and Corresponding Shipping Weights (kg)			
Front suspension (one corner)		Rear suspension (one corner)	
Hub Assembly	2.3 kg	Hub Assembly	2.4 kg
½ of Front Axle	4.2 kg	Knuckle	6.4 kg
Steering Knuckle	3.7 kg	Strut Assembly	4.8 kg
Strut Assembly	4.4 kg	Brake Drum	4.4 kg
Disc Brake Rotor	6.3 kg	Drum Shoes	1.0 kg
Brake Caliper and Pads	2.9 kg	Brake Hardware	0.8 kg
½ of Control Arm	2.2 kg	Wheel Cylinder	0.5 kg
		½ of Bottom Control Arm	0.6 kg
Total	26 kg	Total	20.9 kg

The stiffness values of the front and rear suspensions were determined respectively to be 41,800 N/m and 31,700 N/m per corner, *e.g.*, the front-right suspension stiffness was 41,800 N/m which was also the value of the front-left stiffness; the total front stiffness was 83,600 N/m and the total rear stiffness was 63,400 N/m. These values were determined by placing a known mass of 53 kg on the sprung body at the front middle and then rear middle of the vehicle; at each placement, the distance between a fixed point on each tire hub and a fixed point directly above on the body of the vehicle was measured using a ruler with millimeter precision. Each measurement was compared with its unloaded value to determine the respective displacement in the suspension. The known added mass and suspension displacement values were assessed with a vertical static force balance to determine the stiffness values of the suspensions. Each suspension displacement for the two different placements is shown in Table 2.

Table 2: Suspension displacement under a 53 kg load.

Placement location	Front Left Displacement	Front Right Displacement	Rear Left Displacement	Rear Right Displacement
Front Middle	8.5 mm	8.5 mm	-3.0 mm	-3.0 mm
Rear Middle	-4.0 mm	-4.0 mm	13.5 mm	13.5 mm

Experimental results from three terrain types are presented in this paper. The three terrains are listed in order from smoothest to roughest: smooth pavement, dirt/gravel terrain, and rough pavement with potholes and cracks. Figure 7 shows frequency responses of the unsprung and sprung mass accelerations that resulted from these three terrain types. The target speeds were 40 km/h (25 mph) for the smoothly paved terrain, 25 km/h (15 mph) for the dirt/gravel terrain, and 40 km/h (25 mph) for the roughly paved terrain.

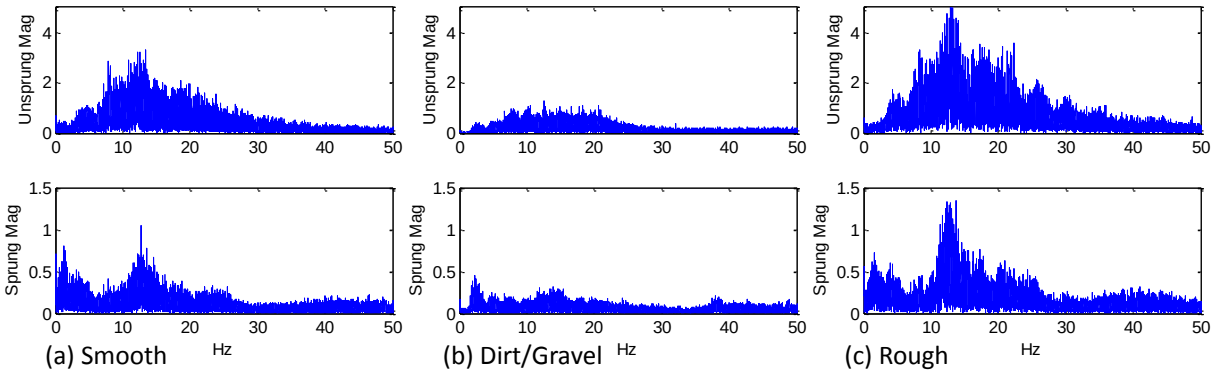

Figure 7: Spectrum of acceleration magnitudes for (a) smooth pavement, (b) dirt/gravel terrain, (c) rough pavement.

Figure 8 shows a frequency response plot of the output (sprung mass) acceleration relative to the input (averaged unsprung mass) acceleration for the dirt/gravel terrain. This plot was obtained by taking the discrete-Fourier transform of the output divided by the discrete-Fourier transform of the input. A Bode magnitude plot (solid line) of the base excitation model, Equation (17), with $m = 1295$ and $B_z = 13000$ is also shown on this graph as a reference. This input-output frequency plot shows a resonance peak between 0.9 – 4 Hz. It also shows increased magnitudes for frequencies above 10 Hz. These large magnitudes in the higher frequency range

are the effect of disturbances not captured by the base excitation model. To reduce the effect of these disturbances on the parameter estimates, this paper applied a second order, low pass filter with a natural frequency of 5 Hz and a damping ratio of 0.7 to filter the sprung and unsprung acceleration signals.

The recursive estimation algorithm based on polynomial chaos theory was applied to the data sets from the three terrains discussed above. The polynomial order was set to be $S = 6$, the bounds on the mass estimate were $800\,kg \leq m \leq 2300\,kg$, and the bounds on the damping coefficient were $4000 \leq B_z \leq 28000$ Ns/m. Figure 9 shows the convergence of the polynomial chaos algorithm for vehicle sprung mass for the different terrain types. For each terrain type, the algorithm converged to within 10% of the true sprung mass value. Assuming convergence within 10% error to be acceptable, these results verify that the proposed method can be used successfully for vehicle sprung mass estimation on both smooth and rough terrain.

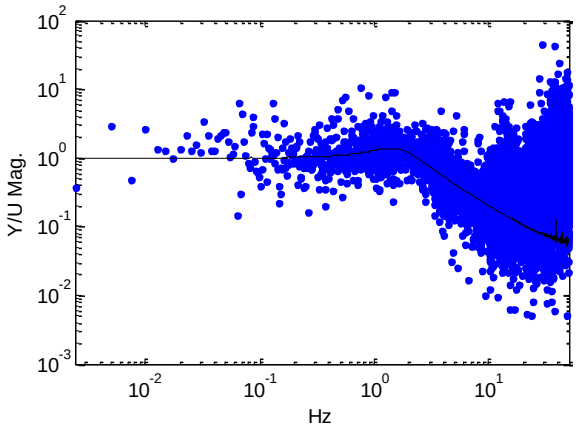

Figure 8: A spectrum of input to output magnitude for the dirt/gravel terrain. Both axes are shown in a logarithmic scale.

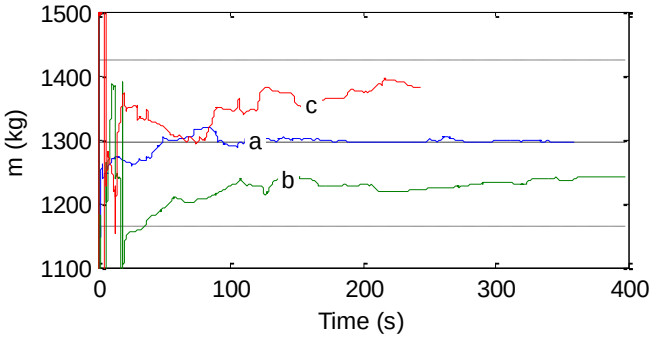

Figure 9: Convergence of the proposed estimator for (a) smooth pavement, (b) dirt/gravel terrain, (c) rough pavement. The dashed line is the true mass value, and the dotted lines are the ±10% error lines.

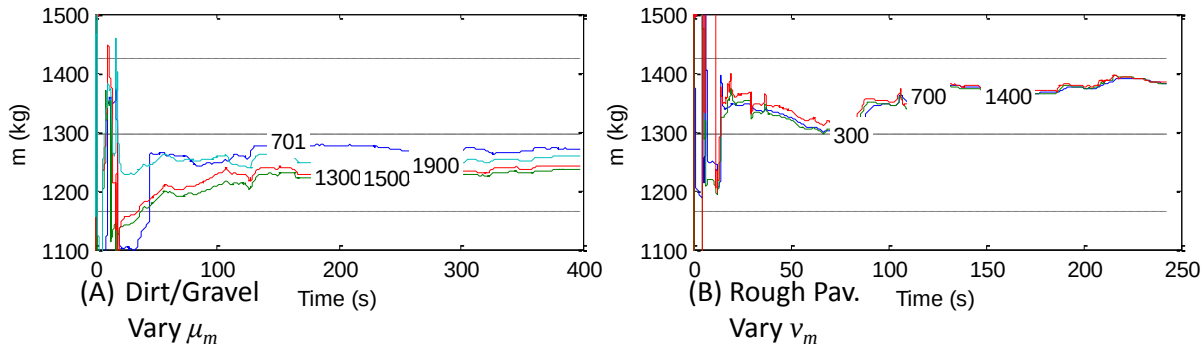

Figure 10: Sensitivity of the polynomial chaos algorithm to varying the value of (A) $\mu_m \in \{701, 1300, 1500, 1900\}$ with $v_m = 700$, and (B) $v_m \in \{300, 700, 1400\}$ with $\mu_m = 1500$. The dashed line is the true mass value, and the dotted lines are the ±10% error lines.

The polynomial chaos algorithm requires a maximum of 6 user defined tuning parameters: the prior mean values μ_m and μ_B, the prior maximum variance values v_m and v_B, the value of the polynomial chaos order S, and the measurement noise variance σ_k. If σ_k is a constant, its value does not affect the parameter estimates. In that case, the polynomial chaos approach is not sensitive at all to the user define value of σ_k. Figure 10 shows the sensitivity of the polynomial chaos algorithm to various prior mean μ_m and variance v_m values.

8 Experimental Comparison with Regressor Methods

Using the same three data sets discussed above, this section compares two regressor methods, Recursive Least Squares (RLS) and Recursive Total Least Squares (RTLS), against the polynomial chaos method discussed in the previous section. The experimental study found that the regressor methods were sensitive to the tuning of the parameters in the user-selected denominator $\Lambda(s)$. In this experiment, the denominator was chosen to be $\Lambda(s) = s^2 + 2\zeta\omega s + \omega^2$. The value of ζ was fixed at $\zeta = 0.0024$ for RLS and $\zeta = 0.707$ for RTLS, and the value of ω was varied between 6 and 12 rad/s (0.95 – 1.9 Hz). Figure 11 demonstrates this sensitivity for the RLS and RTLS approaches using the dirt/gravel terrain data.

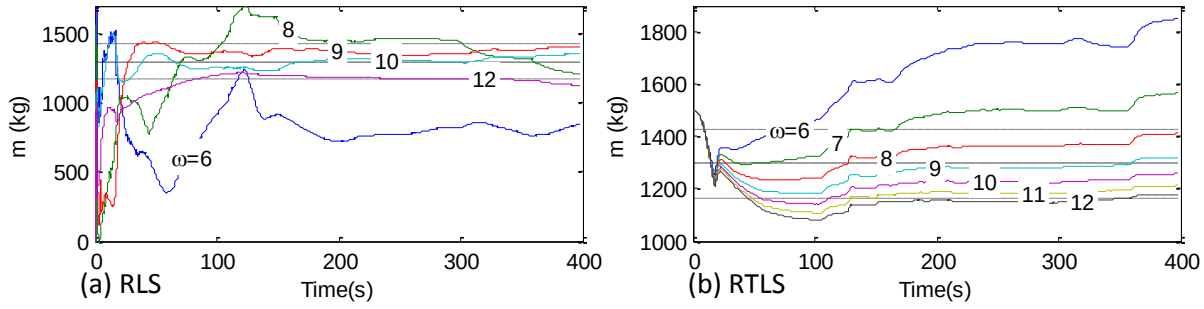

Figure 11: Sensitivity of varying ω for (a) RLS and (b) RTLS approaches for the dirt/gravel terrain. The dashed line is the true mass value, and the dotted lines are the ±10% error lines.

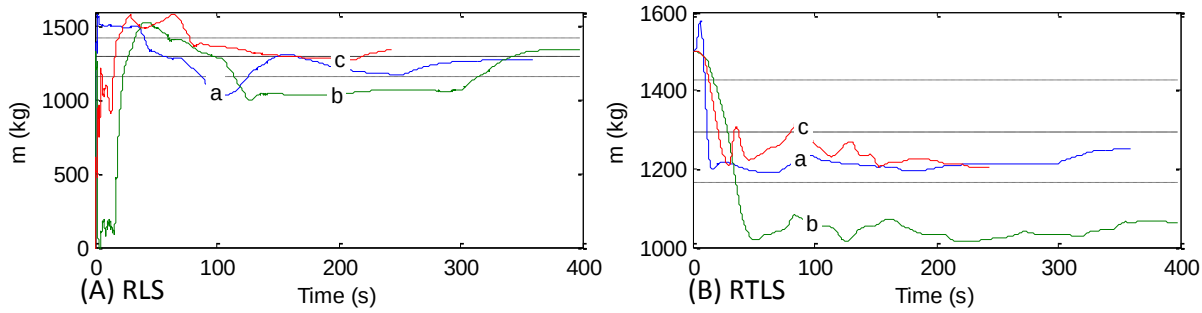

Figure 12: The convergence of the (A) RLS and (B) RTLS estimators for (a) smooth pavement, (b) dirt/gravel terrain, and (c) rough pavement. The dashed line is the true mass value, and the dotted lines are the ±10% error lines.

The next experimental study demonstrates that the optimal (in the mean square sense) tuning of $\Lambda(s)$ for one terrain type is not necessarily optimal, or even appropriate, for another terrain type. The optimal values of ω and ζ for the rough pavement data were found using the optimization algorithm FMINSEARCH in Matlab® version 2008a. For the RLS algorithm, the optimal values were $\omega = 8.44$ and $\zeta = 0.0024$. For the RTLS algorithm, the optimal values were $\omega = 15.4$ and $\zeta = 0.105$. Figure 12 shows the convergence of the algorithms for the three terrain types using these estimator tuning values. Although these values are optimal for the rough pavement, comparing Figure 12 with Figure 11 reveals that they are not optimal for the dirt/gravel terrain, and they are even outside of the ±10% error lines.

9 Experimental Comparison with Filtering Methods

This section applies two filtering methods, the Extended Kalman Filter (EKF) and the Unscented Kalman Filter (UKF) to the three data sets discussed above. Similar to the regressor methods, the filtering methods can be difficult to tune, especially considering the fact mentioned above that they each require at least 25 scalar values to be tuned. As an example, Figure 13 shows the sensitivity of these tuning methods to the value of the measurement error variance. Despite the difficulty, the EKF and UKF algorithms can be tuned to converge to estimates that are nearly identical to those produced by the polynomial chaos maximum likelihood approach. This is shown in Figure 14.

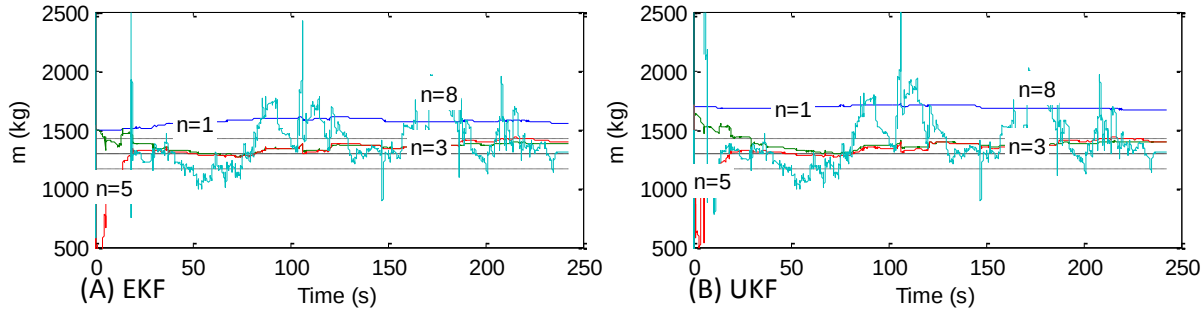

Figure 13: Sensitivity of the (A) EKF and (B) UKF estimators for different values of noise variance = $7 \cdot 10^n, n = 1, 3, 5, 8$.

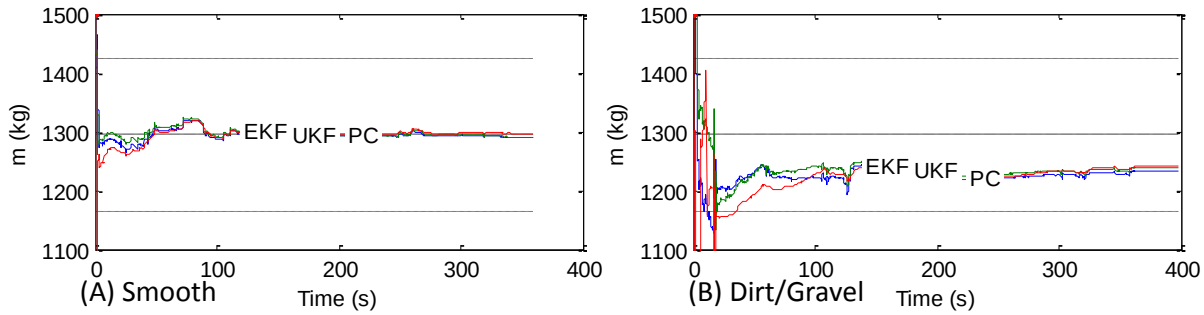

Figure 14: Convergence of the EKF, UKF, and polynomial chaos (PC) methods for (A) smooth pavement and (B) dirt/gravel terrain.

Since the EKF algorithm is more computationally efficient than the polynomial chaos and UKF algorithms, when computational resources are limited, the polynomial chaos approach can help to tune the EKF algorithm offline, and then the EKF algorithm can be implemented online.

10 Conclusions

This paper has introduced recursive techniques for sprung mass estimation of vehicles on rough terrain. It proposed a base excitation model that treats vertical unsprung accelerations, instead of the terrain profile or a suspension actuator, as the input to the estimation model. The experimental results demonstrated that the proposed method is viable for vehicle sprung mass estimation for vehicles driving on rough (and relatively smooth) terrain. No prior knowledge of the terrain profile was required, and no active/semi-active suspension was required. The polynomial chaos approach was compared with regressor model approaches and filtering approaches. The regressor methods are concluded as not appropriate for this sprung mass estimation approach because of their sensitivity to tuning parameters. The filtering methods were also more difficult to tune than the polynomial chaos approach, but they could be tuned to converge to nearly the same estimates produced via the polynomial chaos approach. Based on these results, the polynomial chaos approach is recommended when sufficient computational resources are available, otherwise the extended Kalman filter is recommended.

Acknowledgments

This research was funded by the U.S. Army TARDEC through its center for excellence in automotive modeling and simulation.

References

Blanchard, E. D., Sandu, A., and Sandu, C. (2009a), 'Polynomial Chaos-Based Parameter Estimation Methods Applied to Vehicle System', *Proc. of the Instit. of Mech. Eng. (IMechE) Part K: J. of Multi-Body Dynamics*, 2010, Vol. 224, No. K1, pp.59-81.

Blanchard, E. D., Sandu, A., and Sandu, C. (2009b), 'Parameter Estimation for Mechanical Systems via an Explicit Representation of Uncertainty', *Engineering Computations. Int.*

J. for Computer-Aided Engineering and Software, 2009, Paper no. EC116060, Vol. 26, No. 5, pp. 541-569.

Blanchard, E., Sandu, A., and Sandu, C. (2010), 'A Polynomial Chaos-Based Kalman Filter Approach for Parameter Estimation of Mechanical Systems', *ASME J. of Dynamic Systems Measurement and Control, Special Issue on Physical System Modeling*, 2010, Paper no. 061404, Vol.132, Issue 6, (18), DOI: 10.1115/1.4002481.

Best, M.C. and Gordon, T.J., (1998), 'Suspension System Identification Based on Impulse-Momentum Equations', *Vehicle System Dynamics*, Vol. 20, No. 6, pp. 354-365.

Fathy, H.K., Kang, D. and Stein, J.L., (2008), 'Online Vehicle Mass Estimation Using Recursive Least Squares and Supervisory Data Extraction', *Proc. of the American Control Conference*, Seattle, WA, USA, 2008, pp. 1842-1848.

Ghanem, R. and Spanos, P., (1991), *Stochastic finite elements: A spectral approach*, Springer-Verlag New York Inc.

Huh, K., Lim, S., Jung, J., Hong, D., Han, S., Han, K., Jo, Y.H. and Jin, J.M., (2007), 'Vehicle Mass Estimator for Adaptive Roll Stability Control', *SAE Technical papers*, paper 2007-01-0820, 2007.

Inman, D.J., (2001), *Engineering Vibration*, 2nd ed., Prentice Hall: New Jersey

Ioannou, P.A. and Sun, J., (1996), *Robust Adaptive Control*, Prentice-Hall, Inc.

Kim, C. and Ro, P.I., (2000), 'Reduced-Order Modelling and Parameter Estimation for a Quarter-Car Suspension System', *Proc. IMechE. Part D: J. of Automobile Eng.*, Vol. 214, No. 8, pp. 851-864.

Kubus, D., Kröger, T, and Wahl, F.M., (2008), 'On-line estimation of inertial parameters using a recursive total least-squares approach', *IEEE/RSJ Int. Conf. on Intelligent Robots and Sys.*, Nice, France, 2008.

Li, L., Sandu, A., and Sandu, C. (2005), 'Modeling and simulation of a full vehicle with parametric and external uncertainties,' in *ASME International Mechanical Engineering Congress and RD&D Expo*, Orlando, FL, 2005, pp. 6-11

Lin, Y. and Kortüm, W., (1992), 'Identification of System Physical Parameters for Vehicle Systems with Nonlinear Components', *Vehicle System Dynamics*, Vol. 20, No. 6, pp. 354-365.

Moon, T.K., and Stirling, W.C., (2000), *Mathematical Methods and Algorithms for Signal Processing*, Prentice Hall: New Jersey, pp. 381-389.

Ohsaku, S. and Nakai, H., 'Sprung Mass Estimation Apparatus', *U.S. Patent* 6,055,471, 2000.

Pence, B.L., Fathy, H.K. and Stein, J.L., (2009a), 'Sprung mass estimation for off-road vehicles via base-excitation suspension dynamics and recursive least squares', *Proc. of the 2009 American Control Conf.*, St. Louis, MI, 2009, pp. 5043-5048

Pence, B.L., Fathy, H.K. and Stein, J.L., (2009b), 'A Base-Excitation Approach to Polynomial Chaos-Based Estimation of Sprung Mass for Off-Road Vehicles', *Proc. of the Dynamic Systems and Controls Conference*, Hollywood, CA, 2009

Pence, B.L., Fathy, H.K., and Stein, J.L., (2010), 'A maximum likelihood approach to recursive polynomial chaos estimation', *Proc. of the 2010 American Controls Conference*, Baltimore, MD, 2010

Pence, B.L., Fathy, H.K., and Stein, J.L., (2011), 'Recursive Maximum Likelihood Parameter Estimation for State Space Systems using Polynomial Chaos Theory', accepted with revisions in *Automatica*, Preprint available at http://www-personal.umich.edu/~bpence/ [accessed 01/03/2011].

Poularikas, A.D., (1999), *The Handbook of Formulas and Tables for Signal Processing*, CRC Press LLC: Boca Raton

Rajamani, R. and Hedrick, K., (1995), 'Adaptive Observers for Active Automotive Suspensions: Theory and Experiment', *IEEE Trans. on Control Sys. Tech.*, Vol. 3, No. 1, pp. 86-93.

Ristic, B., Maskell, S. and Gordon, N., (2004), *Beyond the Kalman filter: particle filters for tracking applications*, Artech House: Boston

Sandu, A., Sandu, C. and Ahmadian, M., (2006a), 'Modeling Multibody Systems with Uncertainties. Part I: Theoretical and Computational Aspects', *Multibody Syst Dyn* Vol. 15, No. 4, pp 373–395.

Sandu, A., Sandu, C. and Ahmadian, M., (2006a), 'Modeling multibody systems with uncertainties. Part II: Numerical applications', *Multibody Syst Dyn* Vol. 15, No. 3, pp. 241-262.

Shimp, S.K., (2008), *Vehicle Sprung Mass Identification Using an Adaptive Polynomial-Chaos Method*, MS Thesis, Virginia Polytechnic Institute and State University, Virginia, USA

Simon, D., (2006), *Optimal State Estimation: Kalman, H_∞, and Nonlinear Approaches*, John Wiley and Sons Inc.: New Jersey

Song, X., Ahmadian, M., Southward, S. and Miller, L.R., (2005), 'An adaptive semiactive control algorithm for magnetorheological suspension systems', *J. Vibration and Acoustics*, Vol. 127, pp. 493-502.

Tal, R. and Elad, S., (1999), *Method for Determining Weight of a Vehicle in Motion*, U.S. Patent 5,973,273.